International Journal of Pressure Vessels and Piping 199 (2022) 104765

Contents lists available at ScienceDirect

International Journal of Pressure Vessels and Piping

journal homepage: www.elsevier.com/locate/ijpvp

Specifics of diagnostics and investigation of material properties in pipes with planar defects

Dmitrii Zhukov [a,b,c], Sergey Konovalov [a,c,d,*], Danhe Chen [a], Alexey Melnikov [c], Irina Panchenko [d]

[a] Nanjing University of Science and Technology, Nanjing, China
[b] Gazprom Transgaz Samara LLC, Samara, Russia
[c] Department of Materials Technology and Aviation Material Science, Samara National Research University, Samara, Russia
[d] Siberian State Industrial University, Novokuznetsk, Russia

ARTICLE INFO

Keywords:
Delamination
Defects of rolling
Intelligent pigging
Metallography
Safety margin
Load distribution

ABSTRACT

The paper presents findings of a study on planar defects formed on the inner surface of gas pipeline metal in the operation process. The diagnostic indicators of a defective section were determined and analyzed using the intelligent pigging data. A broad range of research was carried out, including visual and measuring control of the object, step-by-step ultrasonic thickness measurement, chemical analysis, optical and electron microscopy, microhardness measurement of defective and defect-free areas, static tensile and impact bending tests. The structure and morphology of defective and defect-free areas were considered. It was determined that the cause of the defects is contamination of the source material with gas pores and fluorspar residues. The defects of planar nature are formed during rolling and can be characterized as metal delamination. The maximum detected thickness of the inclusions was 1.0 mm, however, the main part was rolled to 10.0 μm. The key feature of defects is their location on various levels throughout the wall cross-sections, ranging from one to four detected layers or groups of rolled discontinuities. It is shown that such defects lead to a change in the strength properties of defective area, uneven distribution of loads and reduction in safety margin of the object.

1. Introduction

The length of main gas pipelines operated in the world exceeds one million kilometers. The USA (485,600 km [1]), Russia (175,200 km [2]) and European countries (142,700 km [3]) are the most advanced in this respect. Explosion and fire hazard, high pressure, significant dependence of electrical power generation and chemical industry on natural gas impose strict requirements on reliability of gas pipelines.

Comprehensive and open statistical data on the operation of gas pipelines in Europe for the fifty-year period [3] demonstrate that from 1970 to 2019 the number of failures and accidents decreased by more than six times. Furthermore, the number of recorded failures since 2010 has been quite stable, ranging from 0.12 … 0.13 per 1000 km in a year. The principal factors responsible for failures are external effects, corrosion, material defects and soil movements. One of the priorities in the further operation of hazardous facilities distributed over large areas, including gas pipelines, is to reduce the number of failures or keep it low.

It is almost impossible to forecast destructive external effects, which periodically cause failures, but their influence can be moderated by organizational measures, restricting the access into protected zones and placing the warning signs. The impact of corrosion damage is investigated in details and the methods of metals protection from corrosion are developed. The branch of science focused on this problem is well structured and represented by a wide range of studies [4–8] and anti-corrosion protection methods [9–11]. Currently, these studies are being continued, and modeling systems are used more frequently to predict the behavior of the objects under study for a further period [12–14].

A number of papers consider difficult to forecast soil movements, which lead to structural failures [15–17]. The highest risk for the operation of hazardous industrial facilities, including gas pipelines, is the combined effect of diverse factors [18,19]. The research into the combined effect of factors is more interesting, and in the future its outcomes will help to reduce operational failures that have remained relatively unchanged over the past decade.

* Corresponding author. Nanjing University of Science and Technology, Nanjing, China.
E-mail address: ksv@ssau.ru (S. Konovalov).

https://doi.org/10.1016/j.ijpvp.2022.104765
Received 3 April 2022; Received in revised form 21 July 2022; Accepted 27 July 2022
Available online 5 August 2022

Fig. 1. Inspected site with a defective pipe.

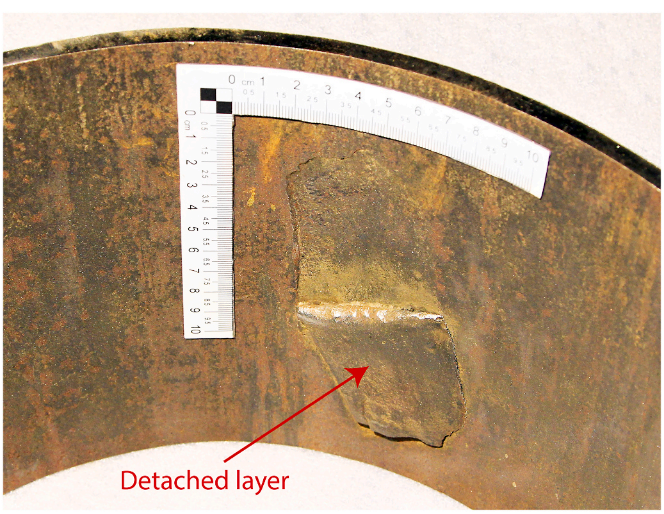

Fig. 2. Delaminated fragment cut out from the pipe.

The most effective inspection technique of long-distance pipeline sections enabling assessment of their technical state is intelligent pigging. Introduction of new technologies, inspection of a wider range of gas pipelines make it possible to detect and eliminate potentially dangerous defective sections. However, it does not completely guarantee trouble-free operation.

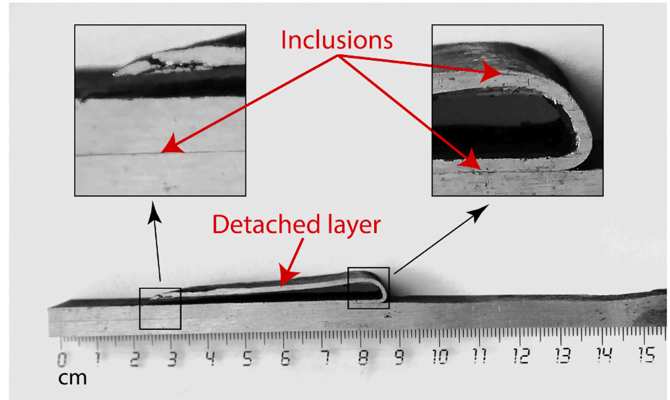

Fig. 3. Delaminated fragment cut out from the pipe.

In recent years, different non-destructive testing (NDT) techniques have been developed for in-line pipeline inspection. The main techniques are magnetic flux leakage (MFL) testing and ultrasonic testing (UT). It should be noted that there are other techniques of in-line inspection, such as electromagnetic acoustic technology (EMAT), eddy current testing (EC), with the additional use of various methods of mechanical or laser profilometry [20–24]. UT is the most accurate technique for controlling the structure and metal defects, but at this stage of development this technique is available for use only with a contact fluid, which can be transported products, for example, oil, products of its processing or other fluids. It is possible to use ultrasonic techniques when filling pipelines with water, however, many associated problems arise, such as the huge required volume, subsequent treatment of the used water and its removal from the pipeline. Therefore, for the control of gas pipelines, MFL techniques are currently preferred as they do not require contact fluids.

This work analyses a defective section of a pipeline containing internal flaws in the pipe metal such as rolled inclusions and gas pores. The area with delaminations is located on the same piping spool, its total length is 5.58 m and it covers approximately 40% of the perimeter.

During intelligent pigging, the anomaly was recorded at a distance of 0.8 m from the weld seam and classified as a technological defect. According to the diagnostic gauge data, its dimensions were 104 × 47 mm. The delamination zone, distributed along the entire length of the pipe and covering approximately 40% of the perimeter, was identified during non-destructive testing of the defective section. The paper compares the results of intelligent pigging with the results of direct non-destructive testing when accessing the inner and outer walls of the pipe. The extended studies of the material physical properties in the defective and defect-free zones, metallographic studies were performed.

The aims of this work are to study the defective section of the pipeline, determine the effect of the changed metal structure on the physical and mechanical properties of facilities, describe characteristic diagnostic features of the defective section obtained during in-line flaw inspection.

2. Materials and methods of research

2.1. Object of research

The object of research is a section of longitudinal electric-welded pipe in the gas pipeline laid underground with the outer diameter of 325 mm and a nominal wall thickness of 8.0 mm. It was operated for more than 25 years and displayed some delamination-type defects (see Fig. 1).

The pipe under study contains internal planar inclusions located along its entire length and directed parallel to the pipe wall. In addition, a number of defects evolved in the operation process. As a result, a

Table 1
Measurement ranges of elements (% mass fraction).

	C	Si	Mn	Cr	Ni	Al	Cu	S	P
Minimum	0.01	0.005	0.002	0.002	0.005	0.001	0.002	0.002	0.003
Maximum	1.6	2.25	2.5	5.5	5.5	1.5	0.8	0.4	0.125

The limits of permissible errors are ± (0.003 … 0.16)% of the mass fraction.

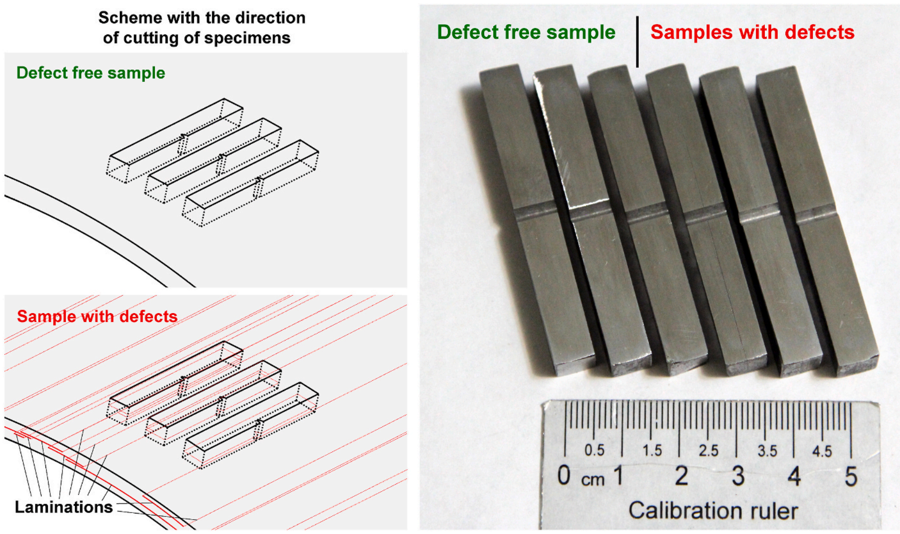

Fig. 4. Samples prepared for impact toughness tests.

fragment of metal delaminated on the inner surface. This delaminated fragment was detected during intelligent pigging; moreover, it was deformed by the pigs (Figs. 2 and 3). The gas pipeline was operated under standard settings with the internal pressure up to 7.5 MPa and inspected with a certain frequency specified by the federal laws of the Russian Federation and PJSC Gazprom standards.

2.2. Analysis of the chemical composition

The chemical composition of the pipe metal was analyzed using an optical emission spectrometer PMI-Master UVR-PRO (WAS AG, Germany) to specify the steel grade and accurately determine the amounts of impurities and alloying elements. The emission spectrometer makes it possible to determine with high accuracy the presence of elements in low-alloy steels in the range presented in Table 1:

2.3. Analysis of the intelligent pigging results

The analysis was focused on results of intelligent pigging, geometry pigging with a pig Relyef-300, magnetic pigging with pigs MDR-300 and MDPR-300 (Russia) of longitudinal and transverse magnetizing.

The geometry pig is equipped with sensors with a polling step of 5.0 mm, the dimensions of the minimum detectable defects are 5 × 10 × 10 mm, determination accuracy of defects location relative to welded seams is 0.5% of the distance. Flaw detectors of longitudinal and transverse magnetization have 160 and 128 sensors, respectively, operating with a step of 4 mm along the longitudinal axis. With a probability of detection (POD) of 90%, the minimum size of a single crack in the base metal is 60 mm with an opening of 0.1 mm, the minimum defect depth is 1.6 mm. The error in determining the length of the crack is ±30 mm.

The intelligent pigging results were compared with the actual parameters of pipes and flaws obtained during examination in the pit and after the defective fragment was cut out.

2.4. Non-destructive control

Visual inspection of the sample was conducted, and the geometrical position, characteristics and dimensions of flaws were specified. A stepwise ultrasonic testing by pulse-echo method was carried out using an automatic flaw detector UMU Skaruch of Scanner series with an acoustic block for thickness measurement No. 129 (Altes LLC, Russia) that includes 4 dual piezoelectric elements 12 × 4 mm in size and operates at a frequency of 4 MHz. Visualization of thickness measurement data and their analysis were conducted by the method described in Ref. [25]. The expanded uncertainty for POD = 95% and a coverage factor equal 2 are estimated ±0.3 mm in all measurement ranges.

2.5. Microstructure analysis

Microsections of samples were prepared for microstructure analysis. Samples 200 mm in length were cut with cooling and prepared using Aka-Clear sample preparation materials (Akasel A/S, Denmark). Polishing was carried out on a metallographic grinding and polishing machine LS2+LSA (Remet, Italy). The microsections were inspected before and after etching in a four percent nital solution. Microsections of the samples were investigated by light optical microscopy with a magnification up to 500× on a binocular optical metallographic inverted microscope METAM LV-31 (JSC LOMO, Russia) and by scanning electron microscopy on a scanning electron microscope TESCAN (Tescan, a.s., Czech Republic) with VEGA software. The elemental composition of metal fragments was investigated by an energy-dispersive tool INCA (Oxford Instruments Analytical, Great Britain).

2.6. Micromechanics tests МикроМеханические испытания

The assessment of mechanical properties along the pipe cross-section required the Vickers hardness measurement performed by HV-1000 microhardness tester (TIME Group Inc., China). For the test sample, the limits of permissible absolute error are ±10 HV.

Table 2
Chemical composition analysis of the pipe material.

	Chemical element									
	C	Si	Mn	Cr	Ni	Cu	Al	S	P	Fe
Defective pipe	*0.214*	*0.281*	*0.534*	*0.07*	*-*	*0.026*	*0.045*	*0.01*	*-*	*98.82*
GOST 1050-88	*0.17 … 0.24*	*0.17 … 0.37*	*0.35 … 0.65*	*< 0.25*	*< 0.3*	*< 0.3*	*-*	*0.035*	*0.03*	*remaning*

2.7. Impact bending tests

The impact toughness was measured by Charpy V-notch test according to GOST R ISO 148-1-2013 "Metallic materials. Charpy pendulum impact test. Part 1. Test method". Three samples with sizes 55 × 7 × 10 mm cut out of defect-free zones and three samples cut out of sections with flaws (Fig. 4) were tested.

Several samples came apart during their preparation and were rejected as defective. The samples, in which the flaws did not cover the entire area, were tested. V-notches 2 mm deep were made mechanically. The tests were conducted using a pendulum impact tester IO 5003-0.3 with an absolute error limit of ±1.5 J. Samples were prepared in cryo-chamber KKM-1M (ZIP LLC, Russia). Before testing samples were cooled to −40 °C. The limit of the permissible value of the error is ±1°C.

2.8. Static tension tests

The static tension tests were conducted as specified in GOST 10006-80 "Metal tubes. Tensile test method" using a tensile testing machine IR 5113-100 (JSC Tochpribor, Russia). Three flaw-free samples as well as eight samples cut out of defective sections were prepared and tested. The samples were prepared as specified for Type II in GOST 1497-84 "Metals. Methods of tension test". The tests were conducted at the ambient temperature of 19°C. The permissible values limits for confidence intervals of the total relative error with a confidence probability $P = 0.95$ are not more than ±1%.

2.9. Finite element modeling

Calculation models were built to determine the effect of various physical and mechanical properties within one pipe on the distribution of strains and stresses in the operated area. The calculation model is represented by a defective pipe, 5 m long, placed between two defect-free pipes, 10 m long. The defective pipe is modeled from two parts having the properties of a defect-free and defective material, respectively. The perimeter length of defective part is 40% of the total perimeter and close to the actually measured on the object. For a comparative analysis, a second calculation model was built, in which there are no defects and deviations in the properties of the considered pipes. The model was constructed and the finite element calculation was performed in the ANSYS environment (ANSYS Inc., USA).

3. Results and discussion

3.1. Analysis of the chemical composition

Table 2 presents the results of pipe metal testing using the PMI-Master UVR-PRO optical emission spectrometer. The testing revealed no deviations in ultimate values of the alloy components; the metal composition corresponds to steel 20 according to GOST 1050-88, as given in the pipe certificate.

Despite the high accuracy of chemical composition analysis, including the carbon content, it should be taken into account that changes in the depth of the object cannot be analyzed in this way. The analysis of the chemical composition was carried out on the outer surface of the pipe.

3.2. Intelligent pigging results

Intelligent pigging, that detected the defective section, was carried out for the first time since the pipeline commissioning. In total, the pigs were pushed through the pipe seven times: four scrapers and three diagnostic pigs.

More than 176 kg of impurities were removed from the gas pipeline by cleaning scrapers, and in addition nearly 50 kg sediments were removed by the diagnostic pigs. The total length of the pipeline amounted to 44.69 km. No emergency situations, blockages of the equipment or ruptures in the gas pipeline were reported. When passing through the pipe under inspection, all three diagnostic pigs detected anomalies in the zone of detached material. The data obtained from pigs of longitudinal and transverse magnetizing were interpreted as local metal losses.

The readings of geometry pig were not matched with the anomalies, since there were no clear evidences of changes in the pipe geometry, and the deviations might have been caused by other factors.

Nevertheless, an obvious diagnostic indicator was obtained when comparing the actual physical configuration of the inner pipe surface after cutting out, the magnetograms from transversal (Fig. 5a) and longitudinal (Fig. 5 b) magnetization with the visualization of the results of geometry pigging (Fig. 5 c), which demonstrated oscillatory movements in the defective zone. Based on the intelligent pigging data this indicator makes it possible to classify clearly the defective zone as a metal delamination on the inner surface accompanied by bending of the detached fragment.

Such flaws were found not very often, so they had no sufficient criteria for identification. The width of the bent metal part was approximately 40 mm with the thickness from 1.0 to 1.5 mm; the bending of the detached part might have been caused by the cleaning scrapers.

3.3. Non-destructive control

Delamination-type flaws were not detected on the outer pipe surface. On the inner surface, the delaminated section 40 mm wide and 80 mm long is bent along the gas flow (Figs. 2 and 3).

The stepwise ultrasonic measurement of thickness was carried out with a step of 2 mm on the entire pipe perimeter over the section with a visible delamination (Fig. 6) and over the adjacent zone at the distance of 300 mm (Fig. 7). The thickness measurement diagrams were plotted to demonstrate the cross-section of the pipe profile. The results revealed that the distribution of multiple flaws along the height of the pipe wall does not allow the presence of delaminations emerging on the inner surface to be to identified with a high degree of certainty. Reflection of signals from overlying flaws does not make it possible to determine the presence of underlying defects or determine the wall thickness containing inclusions. In this case a slightly higher defectiveness degree of a pipe sector with surface delaminations can be determined indirectly. In the zone without surface delaminations there are points with measurements passing the entire wall thickness (Fig. 7). Since delamination defects throughout the wall thickness were not detected by the magnetic pig-assisted method, a surface delamination inside the pipe can be found only by the radiographic testing without the direct access to the inner surface. However, this testing will reveal defects only with the clear

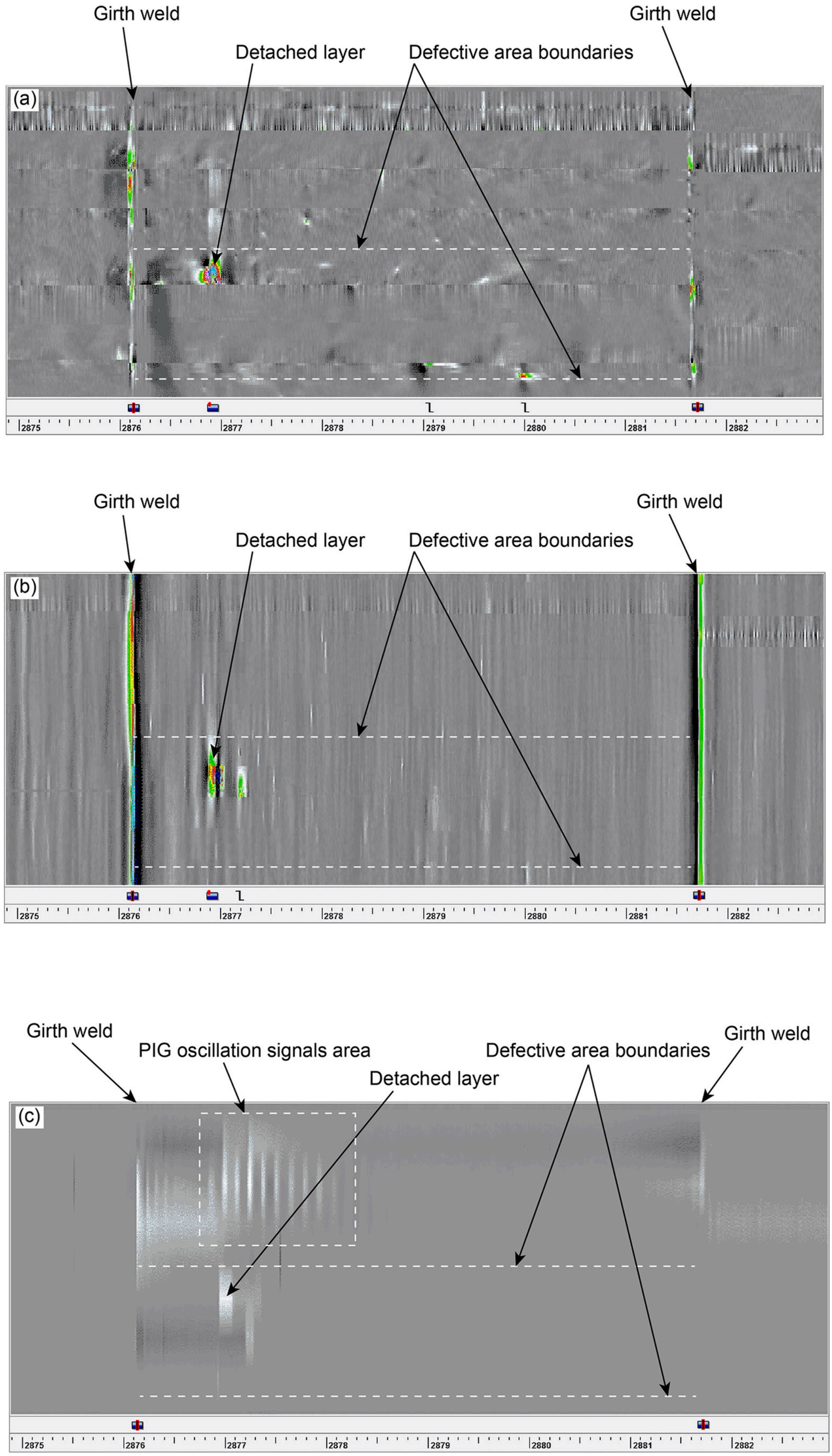

Fig. 5. Results of intelligent pigging (a – magnetogram of the transversal magnetizing pig, b – magnetogram of the longitudinal magnetizing pig, c – visualization of the geometry pig data).

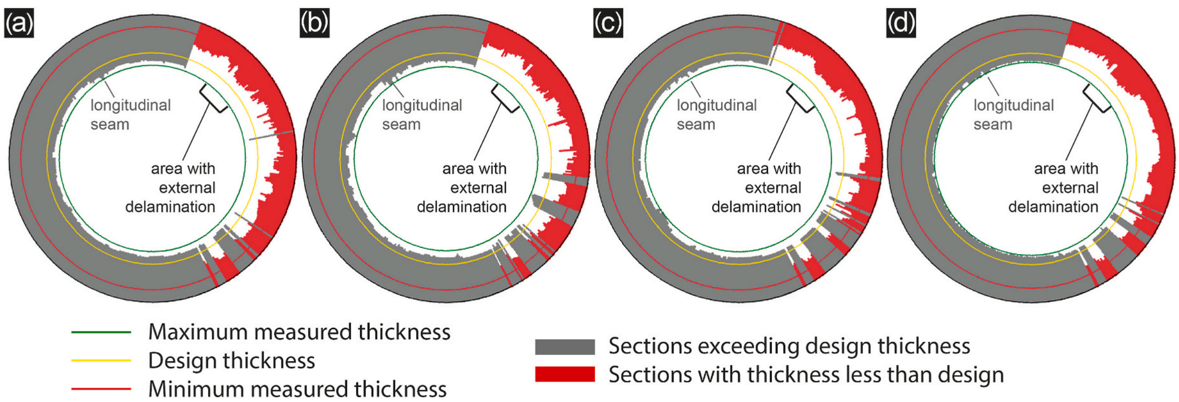

Fig. 6. Results of stepwise thickness measurements above the zone with external delamination (a, b, c, d – thickness measurement diagrams from ultrasonic sensors 1, 2, 3, 4, respectively).

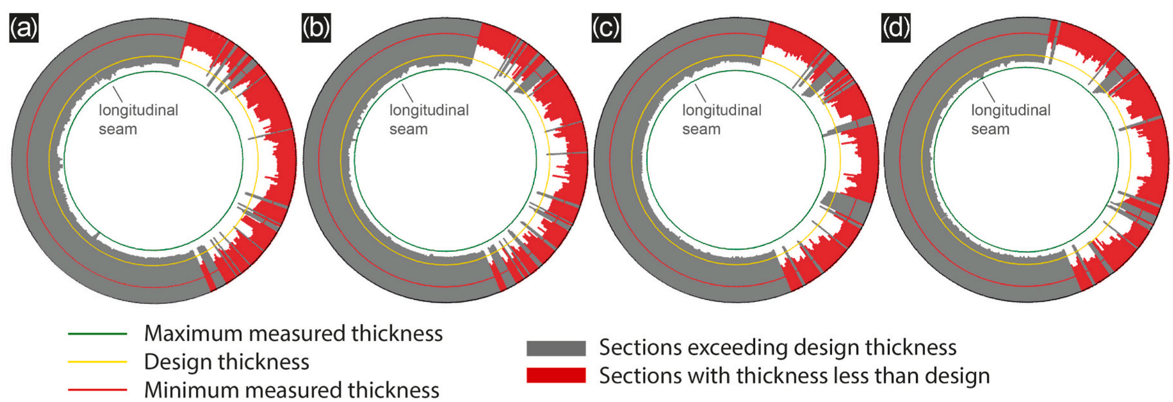

Fig. 7. Results of stepwise thickness measurements above the zone without external delamination (a, b, c, d – thickness measurement diagrams from ultrasonic sensors 1, 2, 3, 4, respectively).

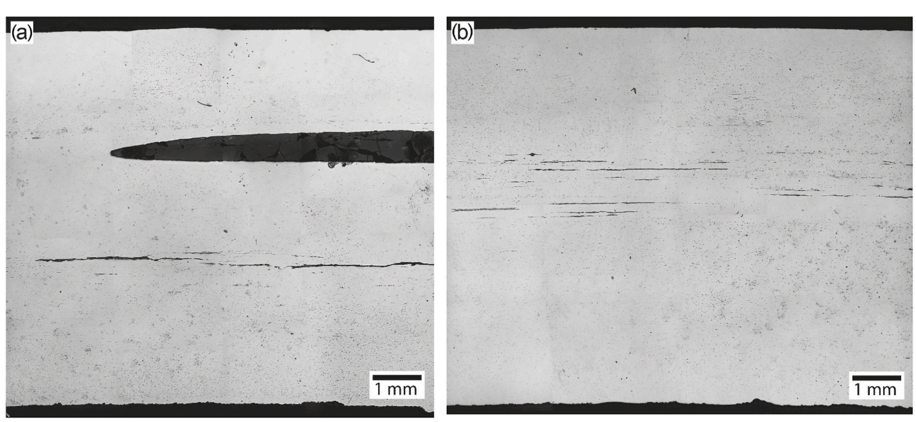

Fig. 8. Optical microscopy of defective zones before etching (a – with significantly thick flaws, up to 1 mm; b – with numerous rolled defects, up to 5 μm thick).

bend of the detached layer. It should be noted that the radiographic testing of long-distance pipeline sections would be cost-and time-intensive. In the case under study, a zone adjacent to delaminations demonstrates a slightly lower density of defects which is expressed in the division of the extended section into several smaller ones. It is emphasized that the detection and hazard assessment of zones with such laminations is now a burning issue necessitating the search for additional solutions [26,27]. Detection and assessment of the danger of such delaminations remains an urgent task that necessitates the search for additional solutions, which is also noted in Ref. [21].

3.4. Optical microscopy

The microstructure of the base metal in samples was analyzed. Multilevel, extended delaminations of various thicknesses were found when examining microsections without etching (Fig. 8).

Areas with chemical inhomogeneity were identified when examining the samples after etching. Namely, an increased carbon content was recorded in the middle part of the pipe, which is confirmed by a higher content of perlite grains.

The defective pipe section exhibits inhomogeneous ferrite-pearlite structure in layers (Fig. 9), moreover, there are delaminations with

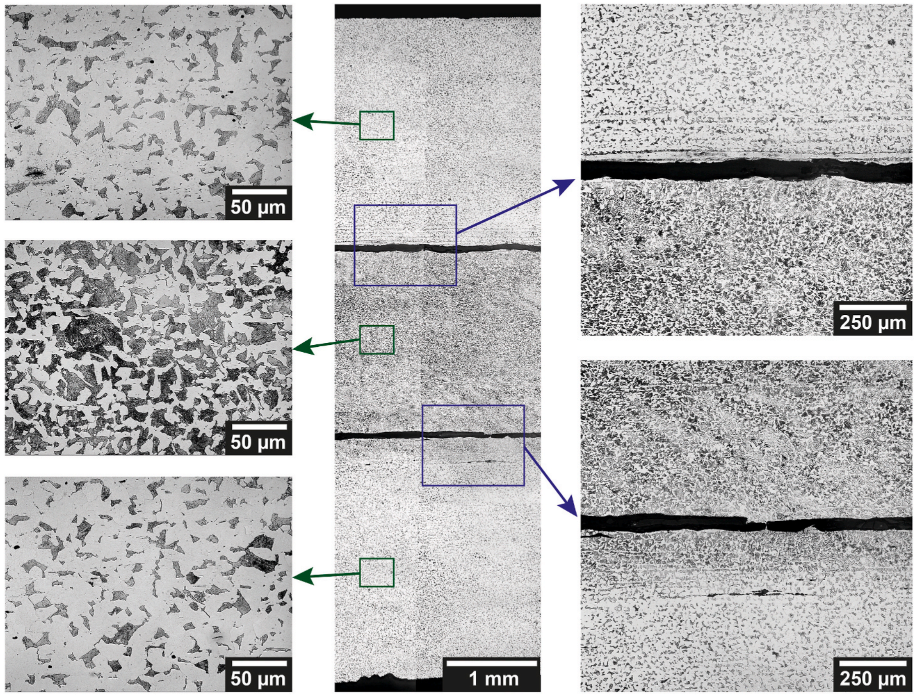

Fig. 9. Optical microscopy of the defective zone with parallel inclusions up to 50 μm after etching.

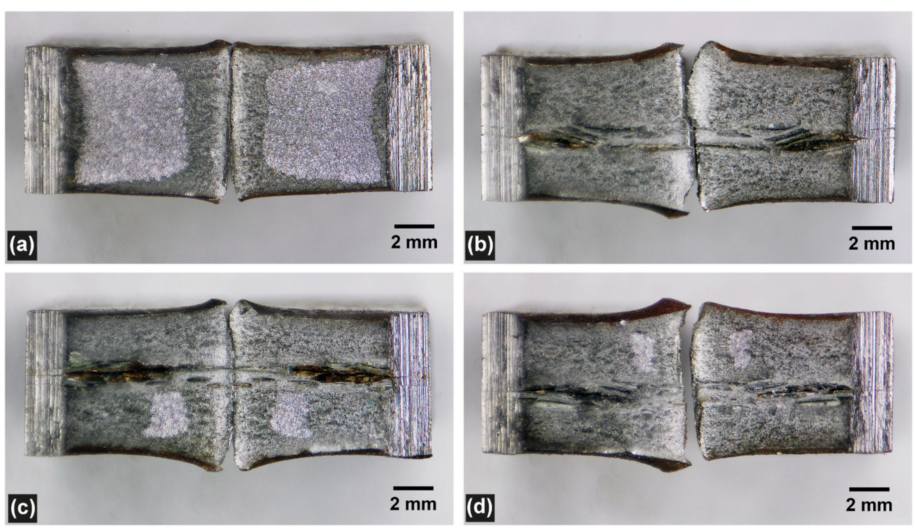

Fig. 10. Macrophotography of fractures in samples (a – defect-free sample, b, c, d – samples with internal flaws).

inclusions from 10 μm to 1 mm in the pipe body. The structure of the defect-free zone has a ferrite-pearlite structure, homogenous throughout the wall thickness, which is typical for low-alloyed hypoeutectoid steels. When determining an amount of carbon by the Rosiwal method during the phase composition analysis, it was established that the percentage of pearlite amounted to 23 … 28% in the defect-free pipe zone, it corresponds to 0.184 … 0.216% of carbon and accords with the steel grade given in the certificate (steel 20 specified by GOST 1050-88). Nearly the same amount of pearlite was detected at the depth of 2–3 mm from both sides of the outer wall surface in the defective pipe. Along the axis of the flaw part there were different structurally inhomogeneous zones, including a stripe-like structure, accumulations of up to three-four ferrite layers and zones with a higher concentration of pearlite. The volume of the pearlite phase, determined by the Rosival method, in such areas reaches 60%, which corresponds to 0.48% of carbon, and goes beyond the permissible limits of the chemical composition of the material used. Steel with a higher carbon content has higher strength properties, but a reduced relative elongation, which should be reflected in the results of mechanical tests.

3.5. Microhardness measurement

The microhardness measurement pointed out significantly different data in defective zones; it is attributed to the chemical inhomogeneity of the inclusions and the metal near inclusions. The microhardness of defect-free samples ranged from 159 to 172 HV0.3/10. The minimal measured microhardness in flaw samples was 152 HV0.3/10, whereas the maximal one amounted to 238 HV0.3/10. Anomalous readings are located closer to the middle of the wall, representing ferrite layers with lower hardness, or local areas with an increased carbon concentration

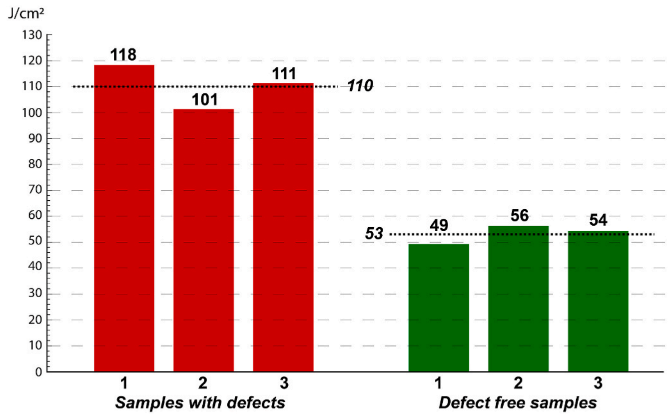

Fig. 11. Results of samples testing.

and pearlite grains, which have a higher hardness. It is also determined that the deviations occupy no more than a third of the wall thickness. Such a deviation of the physical characteristics, to the greatest extent, should affect the characteristic of the relative elongation of the samples during tensile tests, however, the presence of inclusions located at different levels along the wall thickness does not allow the results to be forecasted unambiguously.

3.6. Impact bending tests

Dynamic notched bending tests are used to detect the tendency of metals to brittle fracture. Impact toughness is a complex parameter showing the strength and plasticity of a material. Generally, such tests are carried out to assess the aging of a pipe material but this parameter is of the same importance for the determining parameters of operated materials, including the role of deviation in the structure. It should be noted that a significant number of studies of the metal of gas pipeline pipes operating under high internal pressure describe a decrease in the impact strength index [28–31]. Studies also show that a change in impact strength occurs on objects with a safety margin of less than 1.6 … 1.8. In Ref. [32] it was shown that with a safety margin exceeding 2.0, internal microplastic deformations are insufficient for microstructural changes in the metal, and the properties of the metal did not change after long-term operation. In Ref. [31], the safety margin of the object was ~1.5, while the impact strength decreased by half as a result of long-term operation.

Structural features of materials also have a significant impact. The material in defective zones has a different structure, number of layers, thickness, length and nature of inclusions, and in the object under study all inclusions are parallel to the rolling plane. Furthermore, chemically inhomogeneous zones were found in defective samples, having a hardness different from that measured in the zones adjacent to the outer and inner surfaces. The notches of samples were made perpendicular to the rolling plane to exclude layers without stress risers.

Studies of multilayer samples [33,34] showed an increase in the impact toughness values, regardless of the direction of made stress risers. The most considerable increase in impact toughness was registered quite expectedly when testing samples notched in the planes parallel to layers. Such augmentation was supported by the blocked crack propagation, e.g. by interfaces of layers without initiated stress risers. For fractured samples containing layers perpendicular to stress risers the impact toughness also increased but for another reason: additional work on opening the inter-layer boundaries. The study of the impact strength of samples with local in-plane defects of industrial rather than artificial nature, additionally having a heterogeneous chemical composition, has been poorly studied. However, the tests

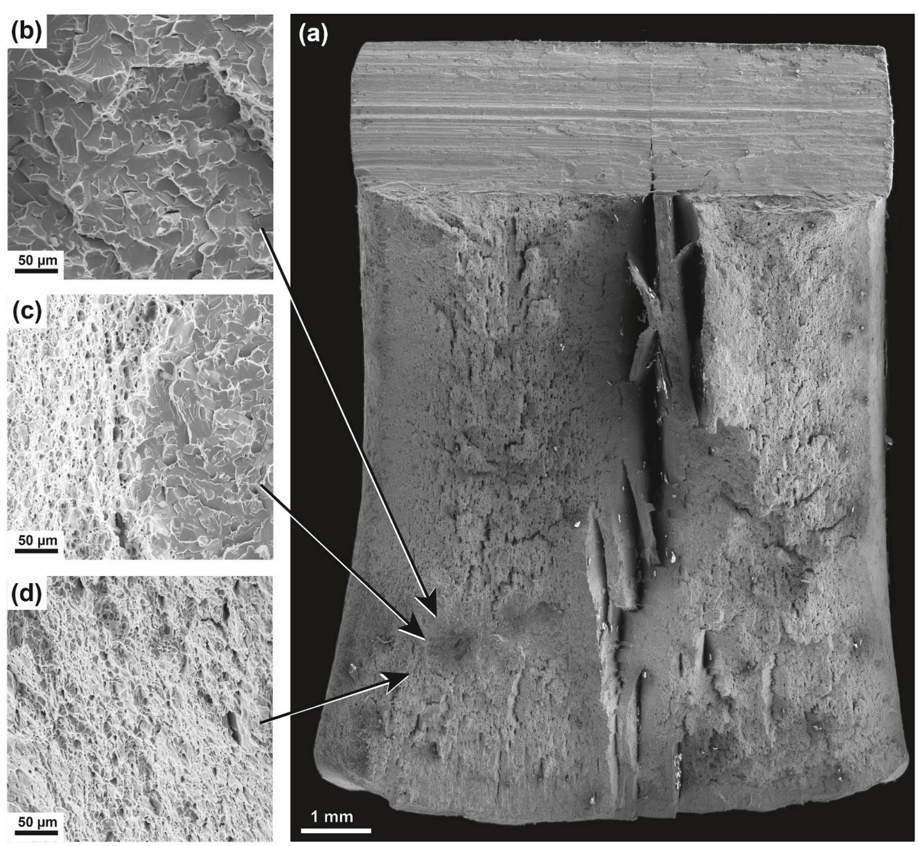

Fig. 12. The defective sample surface after impact toughness tests (a – surface appearance; b – zone of brittle rupture; c – zone with the brittle and viscous fracture boundary; d – zone of viscous fracture).

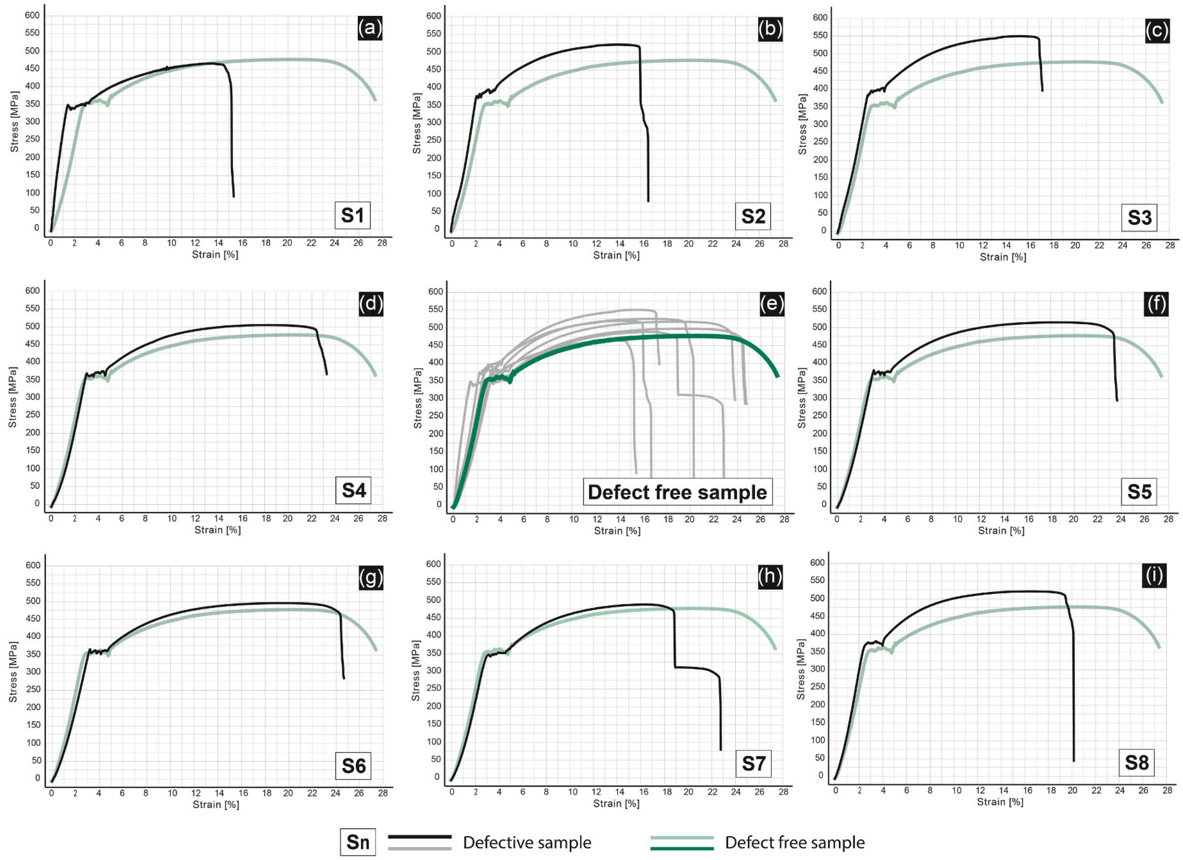

Fig. 13. Tension diagrams based on the test results (a-d, f-i – test results of defective samples in comparison with the flaw-free ones; e – test results of the defect-free sample).

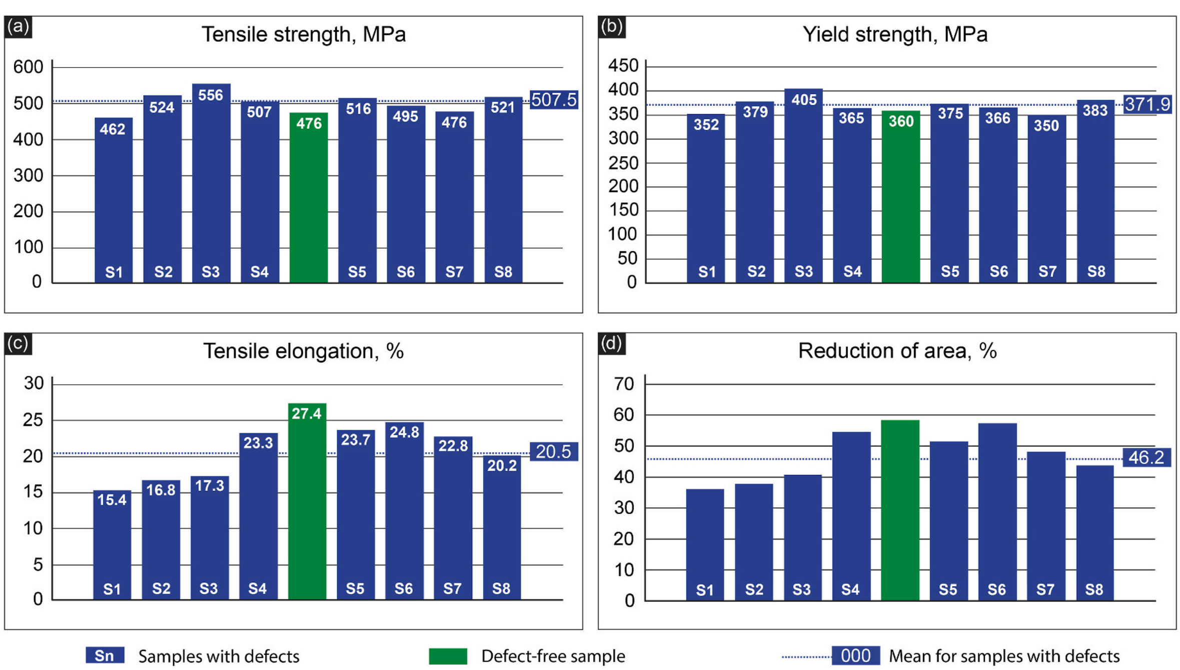

Fig. 14. Consolidated test results (a – tensile strength; b – yield strength; c – tensile elongation, d – reduction of area).

carried out in this work revealed good agreement with the tests results of artificially created layered samples.

Defect-free samples in the analysis of fractures showed a characteristic fracture structure for low-carbon steels (Fig. 10 a). The surface has a viscous fibrous zone and a brittle zone, as well as a rupture area on the opposite side of the zone adjacent to the notch and shear lips on the edges of samples.

The defective samples differ from the defect-free ones by the

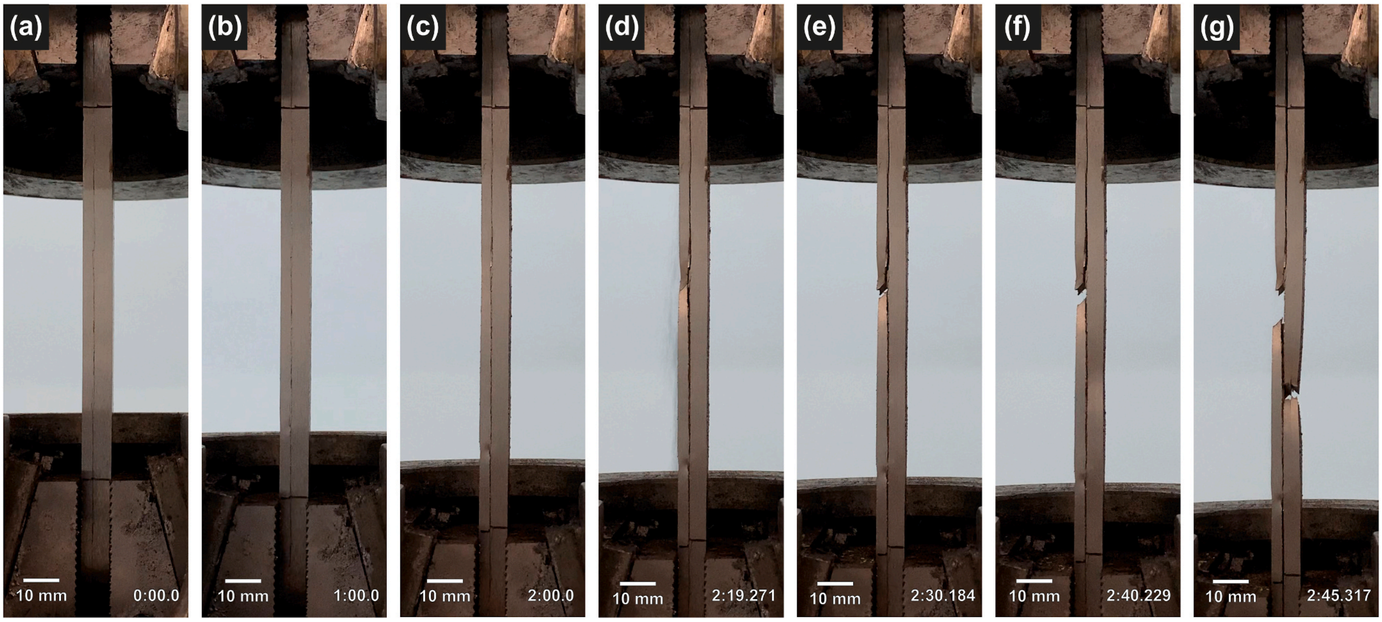

Fig. 15. Fracture dynamics of sample S7 containing layers with different characteristics.

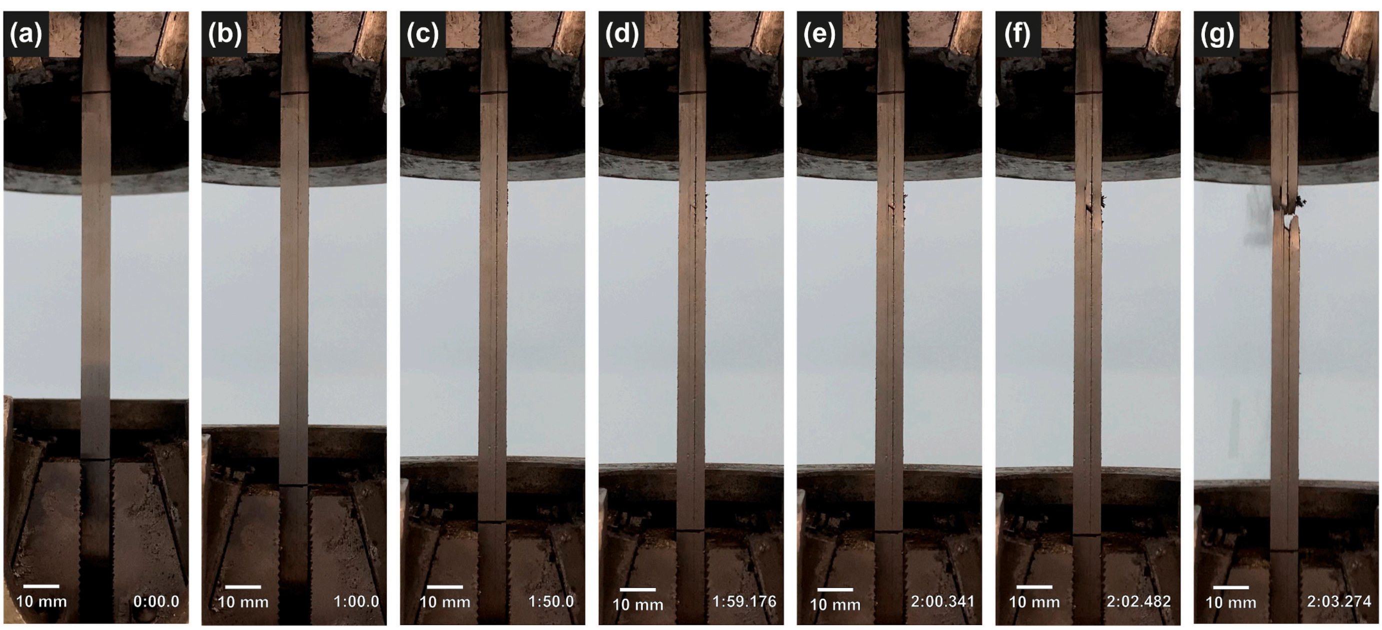

Fig. 16. The fracture dynamics of sample S8 with inner delaminations.

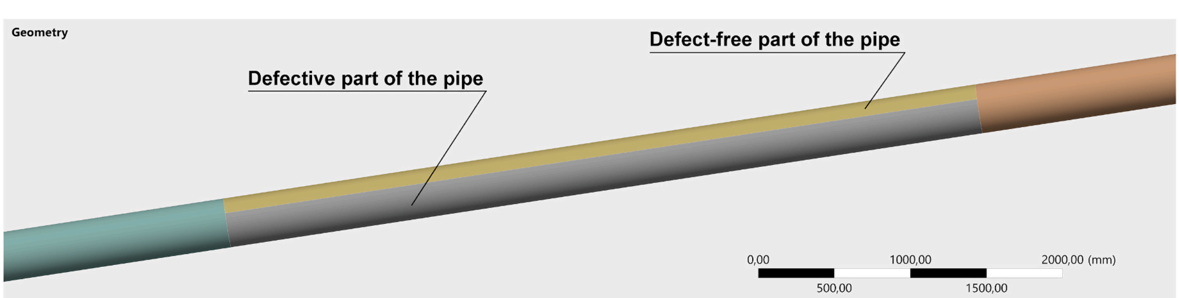

Fig. 17. Geometry of the modeled section.

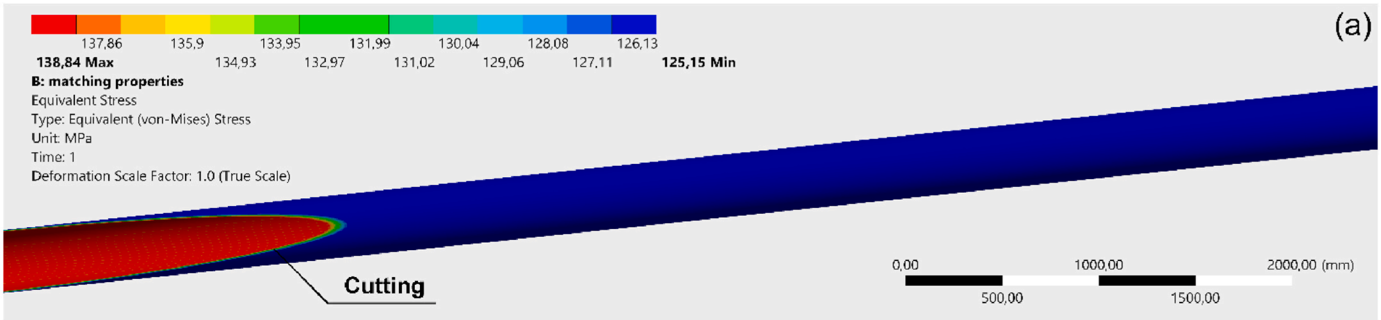

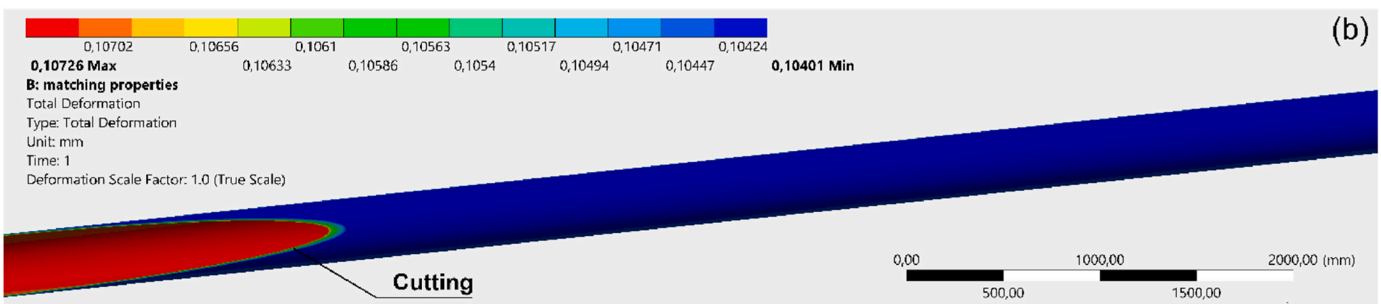

Fig. 18. Defect-free section (a – equivalent stress; b – total deformation).

heterogeneity of surfaces and a reduced or even non-existent brittle rupture zone. The defective zones in the form of thin longitudinal inclusions significantly increased the impact toughness. The samples with inclusions demonstrate a reduced (Fig. 10 c, d) or non-existent (Fig. 10 b) brittle rupture zone.

Inner discontinuities with the maximal thickness up to 50 μm, which are not connected with each other, caused a significant increase in viscous component during testing. An average value of impact toughness in defective samples was almost twice higher that in the defect-free ones (Fig. 11).

3.7. Electron microscopy

An X-ray microanalysis of flaw zones was conducted and reported in Ref. [35]. It revealed that inclusions are of different origins and contain mainly fluorite residues and rolled gas bubbles. Electron scanning microscopy of the defective sample surface was carried out after impact toughness tests. The sample presented in Fig. 12 was analyzed; its macro-photo is given in Fig. 10 d. The small zone has a brittle, transcrystalline fracture structure (Fig. 12b), surrounded by the surface with a fractured fibrous structure (Fig. 12d). Zones with intercrystalline fractures were not detected in samples; this fact confirms that there is no intergranular segregation of harmful particles or steel aging with carbide precipitation along the grain boundaries.

3.8. Static tension test

Static rupture tests (Figs. 13 and 14) were carried out using 11 prepared samples. Eight samples were cut out of defective zones, and three samples were taken from a defect-free zone. The test results of defect-free samples demonstrated slightly different parameters, which characterize low-carbon pipe steels; the deviations were within a statistical error and did not exceed 1.5%. An averaged result was taken as a basic flaw-free sample.

Defective samples fracturing showed that the metal properties changed significantly because of the chemical heterogeneity and inner interfaces. The tensile strength and the yield strength slightly increased by 6.6% and 3.3%, respectively. Flaws had the strongest effect on tensile elongation which decreased by 25.2% on average.

The effect of defects was most pronounced on the sample S7 (Fig. 15), where the material during testing was divided into two zones, with significantly different characteristics and rupture points distant from each other. The sample also clearly shows an additional area of thinning of the layer fractured first and located in the lower part of the sample.

The other samples demonstrated almost similar fracture dynamics: separation into layers and their nearly simultaneous fracture. The typical model of fracture dynamics is presented on the example of sample S8 (Fig. 16). The sample has one visible extended layer. However, defects located along the same axis during elongation merge and additional defective lines are revealed (see Fig. 17).

The middle part of a sample fractured (Fig. 16d) but edge parts bear load for some period of time and resist fracture. The final fracture zone is detected nearly on the same level (Fig. 16 g).

All samples except for S1 demonstrated a slightly increased tensile strength if compared with the flaw-free samples. Sample S1 exhibited a decreased tensile strength due to deeper, up to 0.5 mm, inclusions found throughout the wall thickness, this fact reduced a real area of the material under study.

3.9. Finite element modeling

Modeling of the stress-strain state of the pipe section was performed taking into account the elastic-plastic properties of the material, the bilinear kinematic hardening option was chosen when modeling the plastic behavior of the material. The real data obtained during the ex-

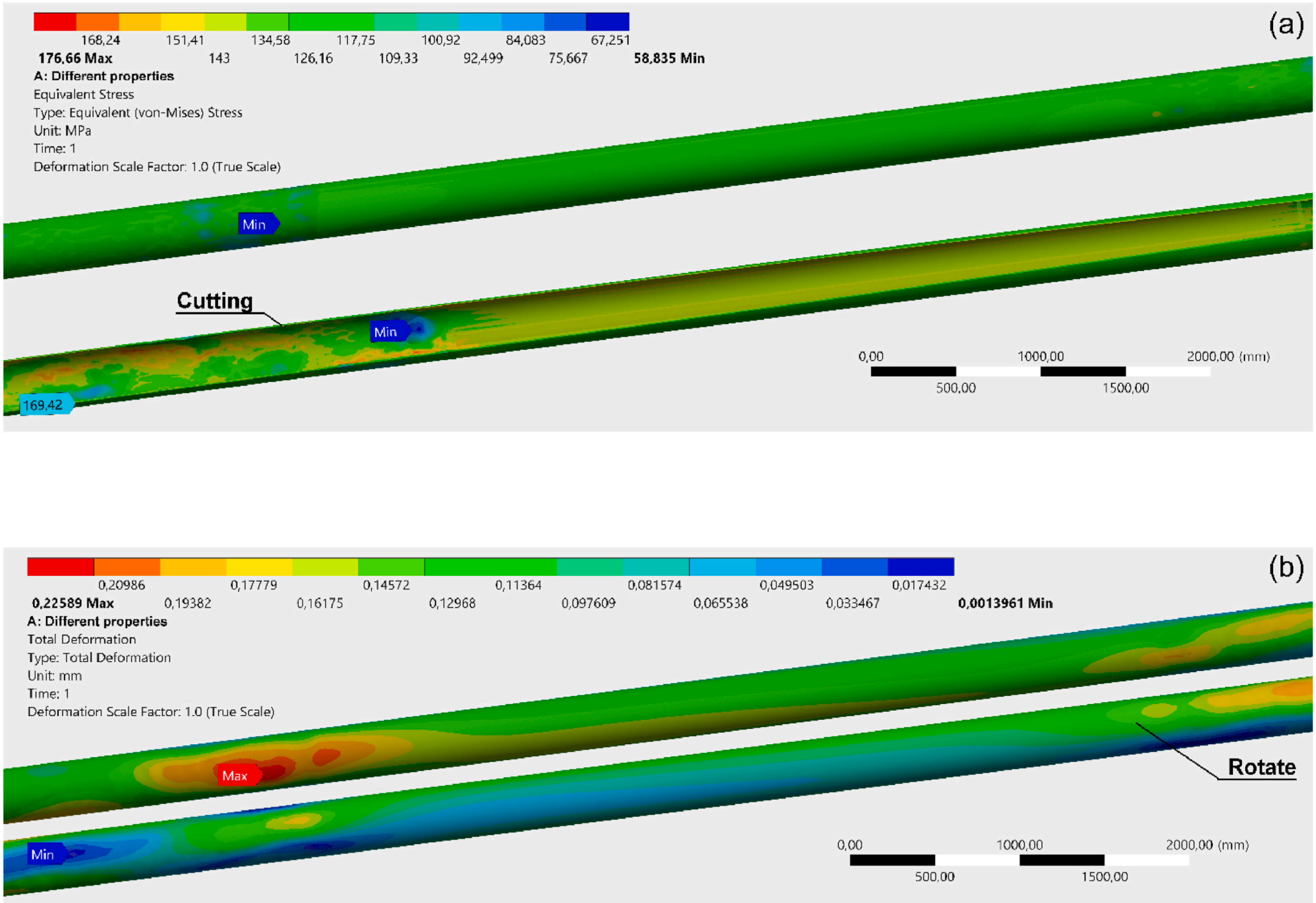

Fig. 19. Modeling of a pipe section consisting of parts with different properties (a – equivalent stress; b – total deformation).

Table 3
Summary of modeling results.

Modeling conditions	Maximum values		Minimum values		Range	
	Stress, MPa	Deformation, mm	Stress, MPa	Deformation, mm	Stress, MPa	Deformation, mm
Defect-free (Fig. 18)	138.84	0.10726	125.15	0.10401	13.69	0.00325
Defective pipe section without internal flaws (Fig. 19)	176.66	0.22589	58.835	0.001396	117.825	0.224494

periments were used to calculate the tangent modulus

$$E_p = \frac{\sigma_t - \sigma_y}{\varepsilon_t - \varepsilon_y} \tag{1}$$

where:

σ_t – tensile strength, MPa;
σ_y – yield strength, MPa;
ε_t – tensile elongation;
ε_y – yield elongation;

In a defect-free material, the tangent modulus is 426.47 MPa, in a defective one – 667.98 MPa.

The deformation distribution gradients of an object with uneven physical and mechanical properties of the material are of considerable interest for determining the behavior of such sections during operation. Numerical experiments showed that the distribution of deformation and stress occurs unevenly when modeling normal operating conditions, represented only by internal overpressure, with heterogeneous metal properties within the same pipe. Summary results are shown in Table 3.

The safety factor of the section is equal to the ratio of the yield strength to the operating stresses in the material:

$$n = \frac{\sigma_y}{[\sigma]} \tag{2}$$

The safety factor of the defect-free section will be 2.59, of the defective section 2.04. Based on the modeling results, it was found that the presence of parts with different physical and mechanical properties of the metal in one pipe leads to a violation of the uniform distribution of stresses and deformation not only in it, but in adjacent areas as well. At the same time, the maximum stresses reaching 176.66 MPa (27% higher than in the defect-free section) occur on the pipes adjacent to the defective one. Sections containing pipes with heterogeneous physical and mechanical properties have a significantly lower margin of safety during operation, in the case under consideration, by 20%.

4. Conclusion

1. The inspection of the internal pipe surface containing delamination and the comparison of results obtained by three diagnostic pigs made it possible to reveal a diagnostic indicator to classify the defect as a

delamination occurring on the inner surface with a bent of the detached metal fragment. This indicator is the coincidence of anomaly zones revealed by magnetic pigs with different directions of magnetization and recording of geometry pig vibrations starting in the zone of their end.

2. The investigation determined that thin, parallel to the surface delaminations, which does not occur on the outer surface, has the most significant effect on the impact toughness because of the increased work on the opening of interlayer boundaries. The change in other characteristics is largely due to the heterogeneity of the physical characteristics of the pipe steel along the wall thickness. However, the presence of defects changes the characteristics of the material in a significant range, and does not allow such sections to be forecasted with high accuracy in the future.
3. Although the defect was detected during intelligent pigging, the use of MFL pigs is ineffective for detecting laminations, which are parallel to the pipe wall and do not occur on the surface. The criterion for detecting this defect was the deviation of the geometry of the pipe surface.
4. Detecting and excluding from operation sections with internal delaminations parallel to the wall require an integrity dig and direct ultrasonic inspection, which are cost-intensive for long-distance subsurface gas pipelines. Further studies need to be carried out to develop methods for the intelligent pigging of gas pipelines, which will significantly increase the effectiveness of diagnostics and reduce the cost of the additional integrity dig.
5. The presence of in-plane defects in pipes leads to a change in the mechanical properties of the defective area and affects the adjacent defect-free areas. In the considered case, the defective area had a slightly increased tensile strength and reduced ductility compared to defect-free zones. It was determined that the disadvantage of objects with such defects is the inhomogeneity of stress distribution even under normal operation conditions. Such deviations, extending to a part of one pipe spool, lead to uneven distribution of loads on adjacent areas causing a general decrease in the safety margin of the object.

CRediT authorship contribution statement

Dmitrii Zhukov: Investigation, Writing – review & editing, Conceptualization. **Sergey Konovalov:** Investigation, Writing – review & editing, Supervision. **Danhe Chen:** Formal analysis, Writing – original draft. **Alexey Melnikov:** Resources, Methodology, Writing – review & editing. **Irina Panchenko:** Resources, Writing – original draft, Funding acquisition.

Declaration of competing interest

The authors declare that they have no known competing financial interests or personal relationships that could have appeared to influence the work reported in this paper.

Data availability

Data will be made available on request.

Acknowledgements

This research was carried out within the framework of the state task of the Ministry of Science and Higher Education of the Russian Federation No. 0809-2021-0013.

References

[1] U.S. Natural Gas. Pipelines. https://www.eia.gov/naturalgas (accessed 14.03.2021).
[2] About Gazprom. https://www.gazprom.com/about (accessed 14.03.2021).
[3] 11th Report of the European Gas Pipeline Incident Data Group (Period 1970 – 2019), 2020. https://www.egig.eu. (Accessed 14 March 2021). accessed.
[4] X. Du, X. Dai, Z. Li, X. Du, H. Shi, J. Wu, H. Lou, X. Feng, L. Zhao, Z. Li, Corrosion analysis and anti-corrosion measures of oil casing of sulfur content gas wells: a case study of Daniudi gas field in the Ordos Basin, Energy Rep. 7 (2021) 1280–1292, https://doi.org/10.1016/j.egyr.2021.02.041.
[5] T. Zheng, Z. Liang, L. Zhang, S. Tang, Z. Cui, Safety assessment of buried natural gas pipelines with corrosion defects under the ground settlement, Eng. Fail. Anal. 129 (2021), 105663, https://doi.org/10.1016/j.engfailanal.2021.105663.
[6] P. Maruschak, V. Dzyura, O. Prentkovskis, I. Lytvynenko, M. Polutrenko, Microdefects of biocorroded pipe steel surfaces and safety assessment of localized stress concentrators, Metals 10 (2020) 852, https://doi.org/10.3390/met10070852.
[7] E.I. Kryzhanivskyi, M.S. Polutrenko, P.O. Marushchak, I.M. Zakiyev, Biocorrosion and localization of degradation processes on the steel surface of a gas main, Mater. Sci. 55 (2020) 683–692, https://doi.org/10.1007/s11003-020-00359-4.
[8] M.A. Vyboishchik, A.V. Ioffe, T.V. Tetyueva, V.A. Revyakin, I.V. Gruzkov, Degradation and failure of pipes from an oil-and-gas pipeline in media with a high content of carbon dioxide and chlorine ions, Russ. Metall. 10 (2020) 1162–1170, https://doi.org/10.1134/S0036029520100328.
[9] YuI. Kuznetsov, A.A. Chirkunov, A.M. Semiletov, Progress in the inhibition of metal corrosion and the prospects of its use in the oil and gas industry, International Journal of Corrosion and Scale Inhibition 8 (2019) 850–881, https://doi.org/10.17675/2305-6894-2019-8-4-5.
[10] M. Askari, M. Aliofkhazraei, S. Ghaffari, A. Hajizadeh, Film former corrosion inhibitors for oil and gas pipelines - a technical review, J. Nat. Gas Sci. Eng. 58 (2018) 92–114, https://doi.org/10.1016/j.jngse.2018.07.025.
[11] S. Ahmed, V. Orth, M. Foley, K. Kottas, C. Teodoriu, Designing in-house cathodic protection system to assess the long-term integrity of natural gas pipelines, J. Nat. Gas Sci. Eng. 94 (2021), 104116, https://doi.org/10.1016/j.jngse.2021.104116.
[12] S.D. Rahmawati, R.K. Santoso, F. Tanjungsari, Integrated CO2-H2S corrosion-erosion modeling in gas production tubing and pipeline by considering passive layer activity, J. Pet. Explor. Prod. Technol. 11 (2021) 3129–3143, https://doi.org/10.1007/s13202-021-01230-1.
[13] R. Heidary, K.M. Groth, A hybrid population-based degradation model for pipeline pitting corrosion, Reliab. Eng. Syst. Saf. 214 (2021), 107740, https://doi.org/10.1016/j.ress.2021.107740.
[14] G. Qin, Y.F. Cheng, P. Zhang, Finite element modeling of corrosion defect growth and failure pressure prediction of pipelines, Int. J. Pres. Ves. Pip. 194 (2021), 104509, https://doi.org/10.1016/j.ijpvp.2021.104509. Part A.
[15] A. Vasseghi, E. Haghshenas, A. Soroushian, M. Rakhshandeh, Failure analysis of a natural gas pipeline subjected to landslide, Eng. Fail. Anal. 119 (2021), 105009, https://doi.org/10.1016/j.engfailanal.2020.105009.
[16] J.Y. Zheng, B.J. Zhang, P.F. Liu, L.L. Wu, Failure analysis and safety evaluation of buried pipeline due to deflection of landslide process, Eng. Fail. Anal. 25 (2012) 156–168, https://doi.org/10.1016/j.engfailanal.2012.05.011.
[17] P.G. Cirimello, J.L. Otegui, L.M. Buise, Explosion in gas pipeline: witnesses' perceptions and expert analyses' results, Eng. Fail. Anal. 106 (2019), 104142, https://doi.org/10.1016/j.engfailanal.2019.08.008.
[18] D.V. Savin, D.V. Zhukov, D.V. Komarov, S.A. Kholodkov, I.S. Vinogradov, Analysis of the causes of destruction of strapping elements of pipeline block valves using numerical modelling, Oil and Gas Territory 7–8 (2021) 90–96. https://tng.elpub.ru/jour/article/view/1380.
[19] P.G. Cirimelloa, J.L. Oteguia, L.M. Buise, Explosion in gas pipeline: witnesses' perceptions and expert analyses' results, Eng. Fail. Anal. 106 (2019), 104142, https://doi.org/10.1016/j.engfailanal.2019.08.008.
[20] Q. Feng, R. Li, B. Nie, S. Liu, L. Zhao, H. Zhang, Literature review: theory and application of in-line inspection technologies for oil and gas pipeline girth weld defection, Sensors 17 (2017) 50, https://doi.org/10.3390/s17010050.
[21] M. Witek, Validation of in-line inspection data quality and impact on steel pipeline diagnostic intervals, J. Nat. Gas Sci. Eng. 56 (2018) 121–133, https://doi.org/10.1016/j.jngse.2018.05.036.
[22] Q. Ma, G. Tian, Y. Zeng, R. Li, H. Song, Z. Wang, B. Gao, K. Zeng, Pipeline in-line inspection method, instrumentation and data management, Sensors 21 (2021) 3862, https://doi.org/10.3390/s21113862.
[23] L.S. Dai, Q.S. Feng, J. Sutherland, T. Wang, S.Y. Sha, F.X. Wang, D.P. Wang, Application of MFL on girth-weld defect detection of oil and gas pipelines, J. Pipeline Syst. Eng. Pract. 11 (4) (2020), 04020047, https://doi.org/10.1061/(ASCE)PS.1949-1204.0000497.
[24] R. Amaya-Gomez, J. Riascos-Ochoa, F. Munoz, E. Bastidas-Arteaga, F. Schoefs, M. Sanchez-Silva, Modeling of pipeline corrosion degradation mechanism with a Levy Process based on ILI (In-Line) inspections, Int. J. Pres. Ves. Pip. 172 (2019) 261–271, https://doi.org/10.1016/j.ijpvp.2019.03.001.
[25] D.V. Zhukov, S.V. Konovalov, Express quality analysis of metal structure based on thickness data, AIP Conf. Proc. 2315 (2020), 040051, https://doi.org/10.1063/5.0036787.
[26] V. Stojmanovski, V. Stojmanovski, B. Stavrov, Examination of laminations in the base material on a section of high pressure gas supply pipeline, in: N. Mitrovic, G. Mladenovic, A. Mitrovic (Eds.), Experimental and Computational Investigations in Engineering. CNNTech 2020. Lecture Notes in Networks and Systems, vol. 153, Springer, Cham, 2021, https://doi.org/10.1007/978-3-030-58362-0_1.
[27] H. Nykyforchyn, E. Lunarska, O. Tsyrulnyk, K. Nikiforov, G. Gabetta, Effect of the longterm service of the gas pipeline on the properties of the ferrite–pearlite steel, Mater. Corros. 60 (2009) 716–725, https://doi.org/10.1002/maco.200805158.

[28] S.V. Panin, I.V. Vlasov, P.O. Maruschak, A.V. Eremin, F. Berto, A. S. Syromyatnikova, A. Vinogradov, Influence of long-term cold climate operation on structure, fatigue durability and impact toughness of 09Mn2Si pipe steel, Eng. Fail. Anal. 102 (2019) 87–101, https://doi.org/10.1016/j.engfailanal.2019.04.036.

[29] S.V. Panin, P.O. Maruschak, I.V. Vlasov, A.S. Syromyatnikova, A.M. Bolshakov, F. Berto, O. Prentkovskis, B.B. Ovechkin, Effect of operating degradation in arctic conditions on physical and mechanical properties of 09Mn2Si pipeline steel, Procedia Eng. 178 (2017) 597–603, https://doi.org/10.1016/j.proeng.2017.01.117.

[30] I.L. Yakovleva, N.A. Tereshchenko, D.A. Mirzaev, A.V. Panov, D.V. Shaburov, Impact toughness and plastic properties of composite layered samples as compared to monolithic ones, Phys. Met. Metallogr. 104 (2007) 203–211, https://doi.org/10.1134/S0031918X07080145.

[31] P. Maruschak, R. Bishchak, O. Prentkovskis, L. Poberezhnyi, I. Danyliuk, G. Garbincius, Peculiarities of the static and dynamic failure mechanism of long-term exploited gas pipeline steel, Adv. Mech. Eng. 8 (4) (2016) 1–8, https://doi.org/10.1177/1687814016641565.

[32] D.V. Zhukov, K.K. Chaplygin, S.V. Konovalov, D. Chen, S.V. Voronin, Subsurface corrosion as the main degradation process of 17GS pipeline steel after 50 Years of operation, Journal of Surface Investigation: X-ray, Synchrotron and Neutron Techniques 15 (4) (2021) 872–876, https://doi.org/10.1134/S1027451021040418.

[33] A.N. Morozova, G.V. Schapov, V.A. Khotinov, V.M. Farber, O.V. Selivanova, Influence of the direction of propagation of the main crack on the fracture mechanism upon impact bending of samples of high-viscous steel with a filamentary structure. Compression region, Phys. Met. Metallogr. 120 (2019) 907–913, https://doi.org/10.1134/S0031918X19090096.

[34] V.M. Farber, V.A. Khotinov, A.N. Morozova, N.V. Lezhnin, T. Martin, Diagnosis of the fracture and fracture energy of high-ductility steels in instrumented impact-bending tests, Met. Sci. Heat Treat. 57 (2015) 329–333, https://doi.org/10.1007/s11041-015-9884-4.

[35] D.V. Zhukov, S.V. Konovalov, A.A. Melnikov, D. Chen, Metallography of non-metallic inclusions in pipe metal and impact assessment of defect structures on non-destructive testing outcomes, CIS Iron and Steel Review 1 (2021) 58–63, https://doi.org/10.17580/cisisr.2021.01.10.